

pubs.acs.org/JPCL Letter

Spectrally Selective Time-Resolved Emission through Fourier-Filtering (STEF)

Anthony V. Sica, Ash Sueh Hua, Helen H. Lin, Ellen M. Sletten, Timothy L. Atallah,* and Justin R. Caram*



Cite This: J. Phys. Chem. Lett. 2023, 14, 552-558



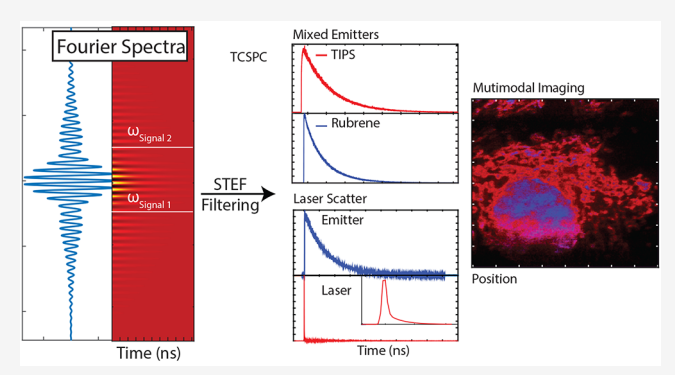
ACCESS I

III Metrics & More

Article Recommendations

s Supporting Information

ABSTRACT: We demonstrate a method for separating and resolving the dynamics of multiple emitters without the use of conventional filters. By directing the photon emission through a fixed path-length imbalanced Mach—Zehnder interferometer, we interferometrically cancel (or enhance) certain spectral signatures corresponding to one emissive species. Our approach, Spectrally selective Time-resolved Emission through Fourier-filtering (STEF), leverages the detection and subtraction of both outputs of a tuned Mach—Zehnder interferometer, which can be combined with time-correlated single photon counting (TCSPC) or confocal imaging to demix multiple emitter signatures. We develop a procedure to calibrate out imperfections in Mach—Zehnder interferometry schemes. Additionally, we demonstrate the range



and utility of STEF by performing the following procedures with one measurement: (1) filtering out laser scatter from a sample, (2) separating and measuring a fluorescence lifetime from a binary chromophore mixture with overlapped emission spectra, (3) confocally imaging and separately resolving the standard fluorescent stains in bovine pulmonary endothelial cells and nearly overlapping fluorescent stains on RAW 264.7 cells. This form of spectral balancing can allow for robust and tunable signal sorting.

 $^{
m extsf{T}}$ ime-correlated single photon counting (TCSPC) uses the emitted photon stream to measure single emitter lifetimes, intensity fluctuations, classical/nonclassical photon correlations,³ and material photophysical characteristics such as the relative polarization, phase, frequency, and time of arrival.^{3,7,8} However, this often involves trade-offs between spectral resolution, throughput, and experiment time, which may limit the ability to resolve complex dynamics in heterogeneous mixtures. Previously we developed Decay Associated Fourier Spectroscopy (DAFS) by utilizing a scanning Mach-Zehnder (MZ) interferometer. DAFS provides the ability to obtain simultaneous frequency and temporal information in the photon stream.¹¹ By avoiding losses and aberrations from monochromator gratings and slits, DAFS retains an optical output mode while concurrently being wavelength agnostic, sensitive to weak signals, and capable of resolving octave spanning signals. However, DAFS is relatively slow, with a typical spectrum requiring ~30 min to collect. To distinguish two signals at different frequencies, the use of specific optical filters is considerably more efficient.

Here we demonstrate that a MZ interferometer can act as a tuned optical Fourier domain filter through judicious choice of the MZ path length difference used to separate any two arbitrary and overlapping luminescence spectral signatures. We implement STEF (Spectrally selective Time-resolved Emission through Fourier-filtering) for several different systems and

show how it can be generalized and extended to applications in microscopy.

Photoluminescence in a Mach–Zehnder Interferometer. In our implementation of MZ interferometry, the incoming photon stream is directed through a beam splitter, separating the light into two paths where we introduce a variable delay (or phase shift) on one path using a retroreflector on a delay stage (Figure 1A); for a more rigorous description, see our previous method paper and Supporting Information (Figure S1). At each output (labeled a and b), we use a single photon avalanche detector (SPAD) to time and measure weak photoemission. The photon stream intensity measured at b (I_b) is subtracted from that measured at a (I_a), recovering a signal proportional to the electric-field first-order correlation function, $g_1(\tau)$. For wide set stationary signals, $g_1(\tau)$ is the real part of the Fourier transform (FT) of

Received: May 18, 2022 Accepted: December 16, 2022 Published: January 11, 2023





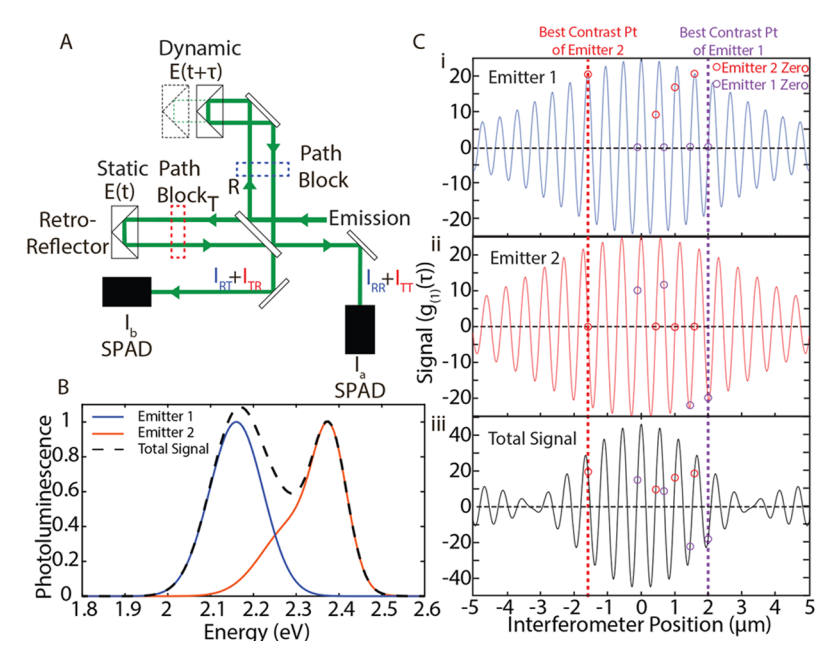


Figure 1. (A) Folded Mach—Zehnder interferometer used for STEF. On one arm, the interferometer scans along a stage position on a dynamic delay stage that defines the interferometer position for Fourier domain filtering, while the other arm remains static. Each path is blocked to record the respective interferometer imbalances. The imbalances are subtracted to recover more efficient filtering of the sample emission. (B) Simulated example photoluminescence spectra of a solution with two spectrally overlapping emitters, blue (emitter 1) and orange (emitter 2) and the sum (dashed line). (C) Real part of the Fourier transform for emitters 1 and 2 and the combined signal. The points where each interference crosses zero are represented by the circles with their corresponding colors. The highest contrast zero-crossing is marked by the dashed lines.

the spectrum of emitted photons, e.g., $\sigma(\omega)$, mathematically represented in eq 1:¹²

$$I_a - I_b \propto \frac{\langle E^*(t)E(t+\tau)\rangle}{|\langle E^*(t)E(t)\rangle|} = g_1(\tau) = \text{Re}\{\text{FT}[\sigma(\omega, \tau)]\}$$
(1)

We plot an example photoluminescence (PL) $\sigma(\omega)$ for two emitters in Figure 1B. 13 In Figure 1C, we plot the FT of the PL spectrum for each emitter individually and the combined signal that would be measured from a mixture. In STEF, the stage position is set to the interferogram zero-point crossing for a particular emitter spectrum. We illustrate this in Figure 1C with the red dashed line, representing a position where emitter 2 is completely canceled out and the combined signal represents signal contribution from only emitter 1. Similarly, emitter 2 can be isolated at the purple lined crossing positions. Red and purple circles represent other positions where emitters 2 and 1 can be canceled, respectively. At any given zerocrossing, we obtain contrast between spectral components through a subtraction of detector signals. As all fluorescent signals have a carrier frequency, STEF can be applied to any line shape and any arbitrary set of two (or more) emitter ensembles provided they have unique zero-crossings.

Finding Zero-Points. Each spectral component's interference pattern has many zero-crossing points. Finding the zero point can be done either by collecting an individual emitter's photoluminescence interferogram and determining the zero-crossing directly or by Fourier transforming a measured individual emitter's photoluminescence spectrum. In our experiments, we used prior knowledge of the emission spectrum of one or both emitters collected through traditional photoluminescence measurements. Once the zero-point crossings are determined, one must select which one to use for spectral filtering. The optimal point will have the highest

contrast, e.g., position with the highest accumulated phase difference between the interferograms of emitters 1 and 2, while also selecting a point that is well separated from the other emitter's zero-points to limit cross-contamination. Thus, the contrast is a function of the carrier frequency and envelope, with narrower signals and different center frequencies leading to optimal contrast. While these considerations are similar to those for normal optical filters, the subtraction of signals allows us to completely cancel out a specific emitter's signal, which is not possible with a single filter and detector. It should be noted that the quality of Fourier filtering is dependent upon the contrast difference in the interferometer. This contrast would be similar if a set of filters were utilized instead because of signal loss that occurs from canonical filtering. We elaborate on this further in the discussion.

Correcting Non-interferometric Imbalances. STEF relies on the cancellation of signals from each output of the MZ interferometer. However, the measured signal difference between each detector may arise due to (i) drift in the interferometer, (ii) differing efficiencies for each detector, and (iii) imperfections in the reflection and transmission of the beamsplitter (or other optical elements after the beamsplitter). Drifting may occur due to thermal fluctuations within the optical elements and/or laser output instability. 13-16 To address drift, we measured our Mach-Zehnder interferometer phase stability over the span of 2 hours, which is longer than a normal STEF measurement. Signals around 380 nm (the shortest wavelength where traditional silicon APDs function, and the worst-case scenario for phase instabilities) corresponded to a 62 cm⁻¹ (7.7 meV) uncertainty in the filtering cut, i.e., two signals must be differentiated at least this much to separate them using STEF in our system. Though this phase shift is very small, it would result in imbalanced subtraction and less complete filtering. (Supporting Information S6).

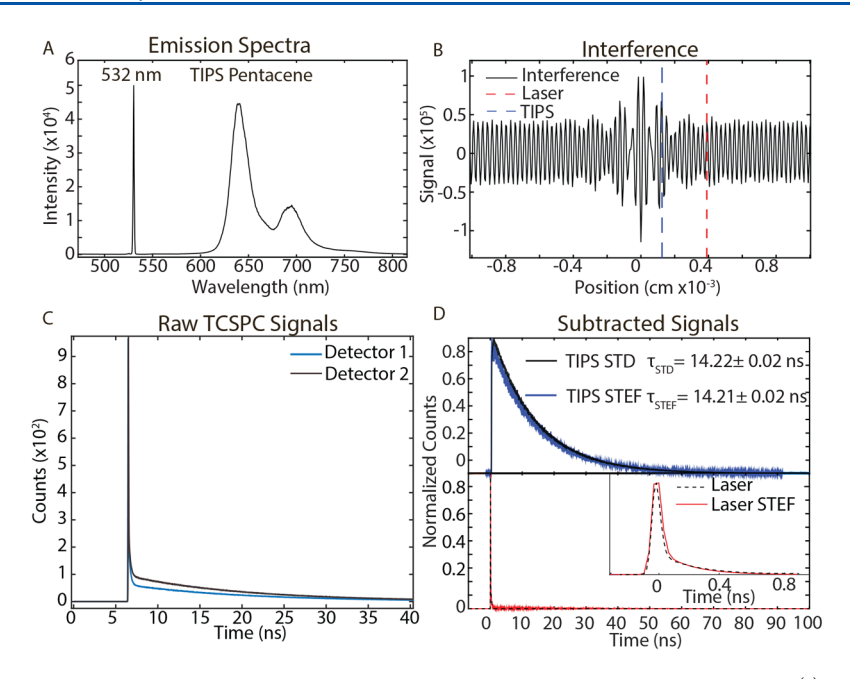


Figure 2. (A) Measured emission spectra of the laser and emitter. (B) Corresponding interferogram $(g^{(1)}(\tau))$ collected with the MZ interferometer. Each dashed line represents the zero-point crossing where either the laser (orange dashed line) or TIPS (blue dashed line) are filtered. (C) TCSPC lifetime from each detector retrieved before balance correction and implementing STEF analysis. (D) After subtraction and correction the signals can successfully separated, yielding the lifetime of TIPS pentacene (top) and the laser limited instrument response function (bottom). The TIPS STEF is compared to the sample's lifetime by itself (TIPS STD). Data is fit to a single exponential.

Further, we note that filtering at the zero-point crossing has the added advantage of balanced detection, where symmetric fluctuations (such as laser drift) cancel out upon subtraction, adding further intrinsic stability to the STEF interferometric methodology.

To correct for detector and optical element imbalances, we perform two simple calibration measurements. We consider the signal measured at detector a/b, which is as follows:

$$I_{a,b} = \frac{\eta_{a,b}}{2} \varepsilon c |E_{a,b}|^2 \tag{2}$$

where $\eta_{a,b}$ are the detector efficiencies, ε is the dielectric permittivity in free space, and c is the speed of light. $E_{a,b}$ are the electric fields at a, b. As the path follows the beamsplitter, we describe the electric field as a series of reflections and transmissions depending on the path:

$$E_a = RRE(t+\tau) + TTE(t) \tag{3}$$

$$E_b = RTE(t+\tau) + TRE(t)$$
 (4)

where τ is the time separation induced by the path length difference. Here we assume that τ reflects a short time difference relative to the decay dynamics of the emitter (Supporting Information S2), and thus the total intensity does not depend on the introduced delay, e.g., $\langle I(t) \rangle = \langle I(t+\tau) \rangle$. We account for our imperfect beamsplitter efficiencies with the R (reflection) and T (transmission) beamsplitter transfer functions $R = \sqrt{\frac{\eta_R}{2}}$ and $T = i\sqrt{\frac{\eta_T}{2}}$ (the i accounts for the $\frac{\pi}{2}$ phase change introduced by the beamsplitter). $\eta_{T,R}$ are the efficiency terms of transmission and reflection, respectively. Putting everything together, we can arrive at the following measured intensity at a:

$$I_{a} = \frac{\eta_{a}}{2} \epsilon c \left[\frac{\eta_{R}^{2}}{4} |E(t+\tau)|^{2} + \frac{\eta_{T}^{2}}{4} |E(t)|^{2} - \frac{\eta_{R} \eta_{T}}{2} E^{*}(t) E(t+\tau) \right]$$
(5)

or

$$\langle I_a \rangle = \frac{\eta_a}{8} \varepsilon c (\eta_R^2 + \eta_T^2 - 2\eta_R \eta_T g^{(1)}(\tau)) \langle I(t) \rangle$$
 (6)

The last term is the first-order correlation function, $g^{(1)}(\tau)$.¹⁷ The same can be done for the second detector:

$$\langle I_b \rangle = \frac{\eta_b}{4} \varepsilon c (\eta_R \eta_T + \eta_R \eta_T g^{(1)}(\tau)) \langle I(t) \rangle \tag{7}$$

To correct for unknown reflection and transmission terms, we block each path of the interferometer (Figure 1A) and measure the intensity at a and b. We denote the intensity upon blocking each respective path as a series of R and T terms. For example, I_{aTT} is the intensity measured at a when the static retroreflector is blocked. Each path can give

$$I_{xyz} = \frac{\eta_x}{4} \epsilon c \eta_y \eta_z \langle I \rangle \tag{8}$$

where x is each detector and y and z are reflection and transmission terms. This gives the intensities of the blocked paths:

Thus, we can simplify eqs 6 and 7 using blocked path intensities and the interference portion

$$\langle I_a \rangle = [\langle I_{aRR} \rangle + \langle I_{aTT} \rangle - \epsilon c \eta_a \eta_R \eta_T g^{(1)}(\tau) \langle I \rangle]$$
 (9)

$$\langle I_b \rangle = (\langle I_{aRT} \rangle + \langle I_{aTR} \rangle + \varepsilon c \eta_b \eta_R \eta_T g^{(1)}(\tau) \langle I \rangle)$$
 (10)

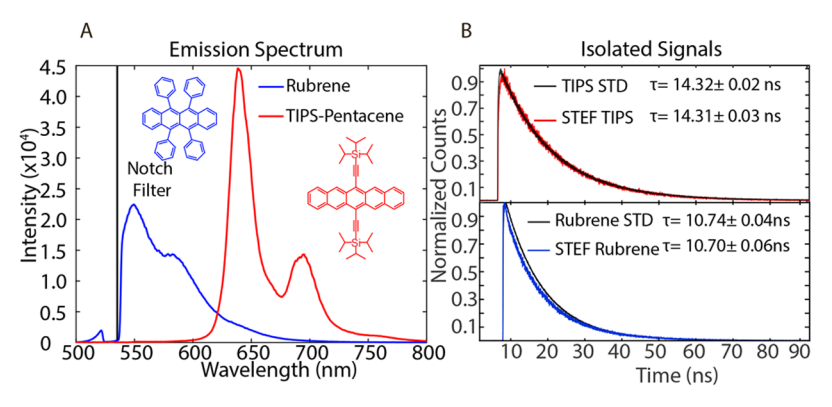


Figure 3. (A) Emission spectrum of the two-emitter system, rubrene and TIPS-pentacene. A 533 nm-notch filter was used throughout the experiment to filter out the laser and maintain a two-component system. The two emitters were excited using a 532 nm-diode laser. (B) Resulting lifetimes from the subtraction of each compared with the lifetimes of each unmixed emitter. The similar lifetimes demonstrate STEF's ability to successfully subtract and isolate emissions, even with molecules of similar lifetimes.

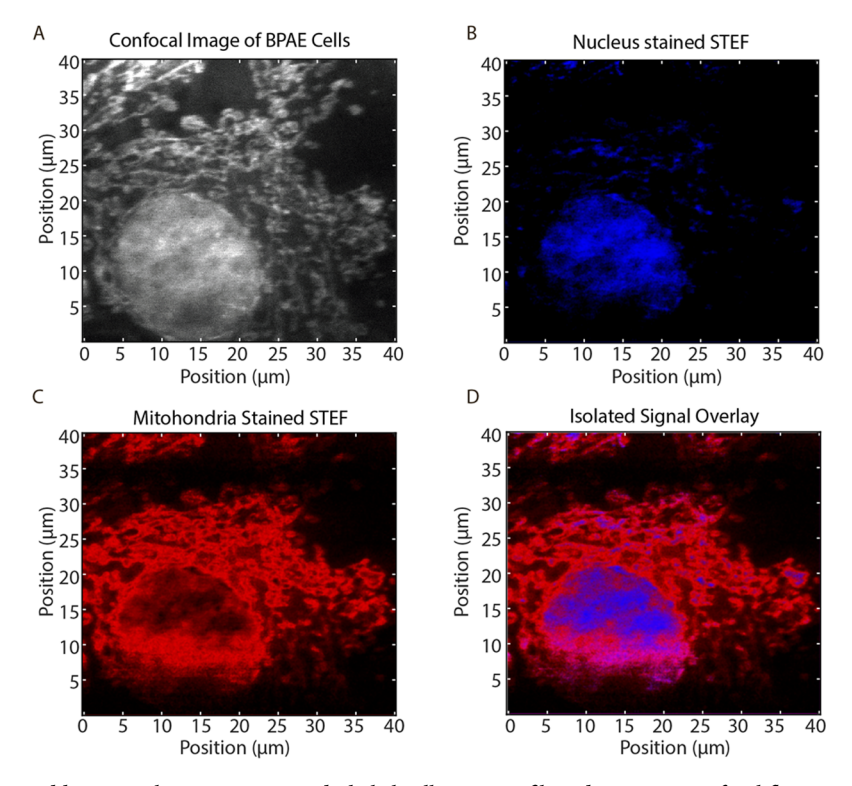


Figure 4. (A) Imaging of stained bovine pulmonary artery endothelial cells using unfiltered scanning confocal fluorescence microscopy. (B) STEF scanning microscope image of nucleus stained with DAPI and with MitoTracker Red CMXRos filtered. (C) STEF scanning microscope image of the mitochondria stained with MitoTracker Red CMXRos and with DAPI filtered. (D) Combined image overlay of the nucleus stained with DAPI filtered emission and mitochondria stained with MitoTracker Red CMXRos filtered emission.

Combining eqs 6 and 7 with the blocked interferometer measurements, the subtraction leaves only the interference terms.

$$\langle I_b \rangle - \langle I_a \rangle - (\langle I_{aRT} \rangle + \langle I_{aTR} \rangle) - (\langle I_{aTT} \rangle + \langle I_{aRR} \rangle)$$

$$= I_{\text{measured}}$$
(11)

$$I_{\text{measured}} = \epsilon c \eta_R \eta_T g^{(1)}(\tau) [\eta_a + \eta_b] \langle I \rangle$$
 (12)

Separating Excitation from Emission. As a proof of principle, we used STEF to separate laser scatter from sample PL (Figure 2). We use TIPS-pentacene (6,13-bis-(triisopropylsilylethynyl)pentacene) in hexane solution with an OD of 0.6. Using a 532 nm pulsed diode laser (LDH-P-FA-

530B PicoQuant), we measure lifetime traces through the MZ interferometer using a pair of avalanche photodiodes (PD050-CTD, Micro Photon Devices). In Figure 2A, we show the spectra of the laser and TIPS-pentacene and in Figure 2B the respective interference collected with the MZ interferometer. The interferometer is set to zero-point crossing (Figure 2B) which filters out the laser (red dashed line) and TIPS-pentacene (blue dashed line) fluorescence signal, respectively. We recorded TCSPC traces with the interferometer open (Figure 2C), the static retroreflector blocked, and the moving retroreflector blocked (Supporting Information S3). After subtraction and correction, the laser and TIPS-pentacene signals were successfully isolated (Figure 2D). As expected, the laser signal matches the instrument response function. The

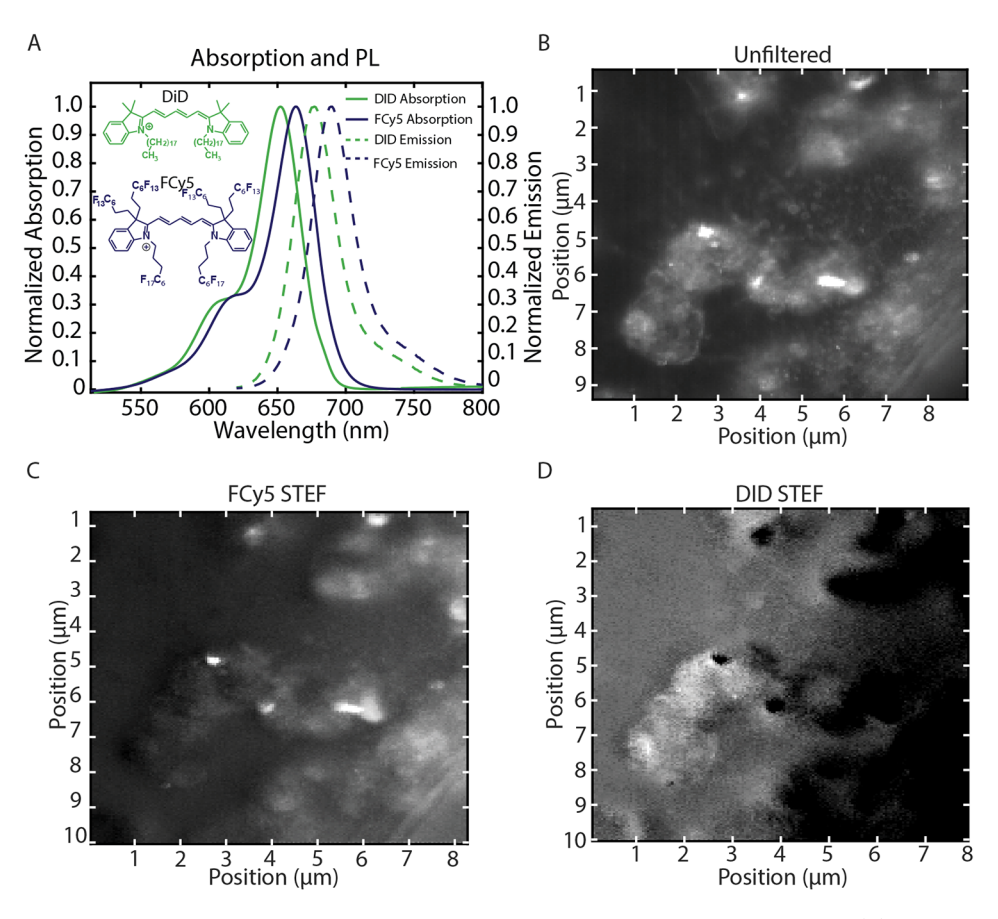


Figure 5. (A) Absorption and emission spectra of DiD and FCy5, where emission peaks are separated by 13 nm. (B) Imaging of stained RAW264.7 cells using unfiltered scanning confocal fluorescence microscopy. (C) STEF scanning microscope image of lysosome stained with FCy5 with DID filtered. (D) STEF scanning microscope image of the membrane DID with FCy5 filtered.

STEF resolved TIPS-pentacene signal is identical to a standard TIPS-pentacene lifetime decay acquired by measuring the lifetime of TIPS by itself in an unmixed system. The TIPS standard and TIPS STEF give equivalent lifetimes. This demonstrates the powerful utility of STEF in filtering out laser scatter, which is often detrimental in imaging and spectroscopic measurements.

Separation of Two Emitters. We next employed STEF in a binary mixture of rubrene and TIPS-pentacene in a hexane solution (Figure 3A) with a similar excitation-collection setup as above, but with an added 533 nm laser notch filter (NF533-17, Thorlabs). TIPS-pentacene and rubrene were used at an absorbance ratio of 0.63:0.57 OD, respectively. This demonstrates the generality of STEF's ability to separate signals of arbitrary spectral shape, even with spectral overlap. We observed the dynamics of each component separately without the use of any additional filters with the exception of a 533 nm laser notch filter. The STEF lifetime traces of the TIPS-pentacene and rubrene mixture components match their single component solution counterparts (Figure 3B) with the exponential fits agreeing within experimental error. This successfully shows the applicability of STEF for mixed chromophore systems.

Separation of Fluorescent Channels in Cellular Imaging. Finally, we show the breadth of STEF's utility by implementing the method in the context of imaging. We performed confocal microscopy to simultaneously image multiple fluorescent channels of stained bovine pulmonary

artery endothelial cells (ThermoFisher, FluoCells Prepared Slide #1). Using a home-built inverted microscope setup (Supporting Information S1) with a piezo stage (Mad City Laboratories Nano-View/M 200-3) and a 100× oil objective (Nikon, Plan APO $100 \times /NA = 1.45$), absolute intensities were collected while scanning across the sample. The scan had a dwell time of 100 ms, resulting in a collection time of 20 min. No filters were used other than a 533 notch filter to block direct laser scatter. Figure 4A shows a confocal image of the sample without any spectral filtering to discriminate the dyestained features. We separated the fluorescence from the DAPI (4',6-diamidino-2-phenylindole) DNA stain (Figure 4B) from that from the MitoTracker Red CMXRos mitochondria stain (Figure 4C) without filters. We first set the interferometer to a zero-crossing point and then performed a confocal imaging scan, with the signal from two detectors summed (Figure 4A). The resulting images from each detector are processed by subtraction to obtain the isolated emissions image from each dye, all from a single experiment. This can be extended to any number of dyes. Each zero-crossing point can be treated as filtering one signal while leaving the ensemble mixed. A careful series of subtractions successfully isolates any desired single emission from a mix of emissions. Figure 4D shows that STEF correctly resolved the blue-stained DNA in the cell nucleus from the surrounding, red-stained mitochondria and allowed for the tuning of whatever signal ensembles appropriate for the system, confirming its general scope in biological or other imaging applications. This approach does not implement timeresolved measurements but could be easily applied for filtering in fluorescent lifetime imaging microscopy (FLIM) measurements. In FLIM, the measurement time can vary depending on the fluence of emitted photons. However, given the brightness of dyes, the dwell time would not change significantly.

As a final proof of principle, a macrophage cell line (RAW264.7) was treated with two heptamethine carbocyanine dyes: DiD (1,1'-dioctadecyl-3,3,3',3'-tetramethylindodicarbocyanine,4-chlorobenzenesulfonate) and FCy5. DiD is a lipophilic fluorophore that associates with membranes and lipid droplets within the cell. FCy5 is a fluorous soluble fluorophore that is introduced by perfluorocarbon nanoemulsions that are internalized by endocytosis and label the endosomes/lysosomes. 18-20 The staining protocol can be found in Supporting Information S5. These dyes had very similar line shapes and emission spectra, with the maxima spaced 13 nm apart (Figure 5A). The zero-point crossing positions were chosen to maximize contrast in the combined signal while maintaining adequate separation between zero crossing points stage positions of the different emitters. The total image (Figure 5B) was obtained in a similar manner as above and while sitting on a singular position. After this, the subtractions obtained yielded a successful separation of FCv5 (Figure 5C) and DiD (Figure 5D). The successful filtering of these two dyes has demonstrated STEF's ability to also separate similar dyes that overlap without specialty filters.

Comparison to Other Methods. Several Fourier domain filtering methods have been previously explored. 13,21-23 Most similarly, Candeo et al. give a complementary interferometric approach for separating fluorescent signals.²⁴ Their method implements the Translating-Wedge-based Identical pulses eNcoding System (TWINS) to direct an emitted photon stream directed through a single-output common-path birefringent wedge interferometer. In their implementation, they collect the emitted photon stream and direct it through the interferometer, imaging at a maxima of the interference pattern. As TWINS is a common path interferometer with minimal moving parts, it offers high stability and accuracy. However, due to the single path and output it forgoes the advantages of a two detector MZ balanced detection scheme. Hence, STEF uses a single measurement to obtain the total binary solution lifetime trace, as well as each individual lifetime component. TWINS can only decrease the signal from one signature without completely canceling it out.

More commonly, optical filter elements such as long, short, and band-pass filters provide a simple method to filter fluorescent signatures. However, these approaches cannot fully cancel a specific spectrum. Designing an analogous filter system would require a beamsplitter which "splits" the spectrum at equal intensity to each detector, which would enable perfect subtraction. Similar approaches have been used to explore spectral diffusion but lack the flexibility of a tunable Fourier domain filter and are limited by the cost and availability of optical components.²⁵ STEF may filter out any arbitrary shape desired by the user including instances of significant spectral overlap. Monochromators with gratings provide some tunability, however, like filters they are limited to selecting spectral bands (by the exit slit) as opposed to spectral shapes. Furthermore, monochromators sacrifice throughput and optical mode for spectral resolution as defined by the grating lines/mm, slit width, and path length of the spectrometer.²⁶ STEF retains the complete sample emission (mode and intensity), allowing for higher throughput and

tunability even at high resolution (0.1 cm⁻¹), dictated by scanning length of the stage. STEF two path/output methodology cancels signals in mixed samples while leveraging the above advantages to acquire isolated signals for lifetimes and imaging as demonstrated above.

Conclusion. As demonstrated, STEF is a powerful tool to separate spectral signatures by leveraging differences in the carrier frequency and coherence length. This avoids difficulties often encountered in systems with emission overlap and complicated line shapes which lead to signal contamination. The practical consideration of STEF's contrast is set by the difference in carrier frequency (or the accumulated phase difference between signals), and their coherence length (the width of the spectrum). Therefore, STEF works best when two signals are separated in energy (carrier frequency) and are narrow (large coherence lengths), paralleling traditional filters. With these factors in mind, STEF presents the advantage of overall tunability and specificity to arbitrary desired signals, working well in cases of overlapping spectral signatures and without requiring specialized filters. It should also be emphasized that STEF leverages the Mach-Zehnder interferometer and only requires two detectors for any number of emitters in solution. Because of this, any mixed sample can be isolated through a series of subtractions with the number of measurements being N-1 where N is the number of emitters. Mach-Zehnder's phase shift sensitivity offers an avenue of advantages including wavelength-range insensitivity, drift-noise cancellation, and optical mode retention. Hence, we were able to demonstrate separation of the emission from a laser and chromophore, two separate chromophores, and imaging of two channels in a stained cellular environment with strongly overlapped spectral signatures. These demonstrations show STEF's wide utility across disciplines in spectroscopy, solution analysis, material science, and biological imaging.

ASSOCIATED CONTENT

Supporting Information

The Supporting Information is available free of charge at https://pubs.acs.org/doi/10.1021/acs.jpclett.2c01504.

Schematic of optical apparatus built for STEF details of STEF setup, application to TCSPC, signals before correction, descriptions of cells and culture conditions, and drift calculations (PDF)

Transparent Peer Review report available (PDF)

AUTHOR INFORMATION

Corresponding Authors

Timothy L. Atallah — Department of Chemistry and Biochemistry, Denison University, Granville, Ohio 43023, United States; orcid.org/0000-0003-2863-6601; Email: atallaht@denison.edu

Justin R. Caram — Department of Chemistry and Biochemistry, University of California, Los Angeles, Los Angeles, California 90095-1569, United States; ⊚ orcid.org/ 0000-0001-5126-3829; Email: jcaram@chem.ucla.edu

Authors

Anthony V. Sica – Department of Chemistry and Biochemistry, University of California, Los Angeles, Los Angeles, California 90095-1569, United States

- Ash Sueh Hua Department of Chemistry and Biochemistry, University of California, Los Angeles, Los Angeles, California 90095-1569, United States
- Helen H. Lin Department of Chemistry and Biochemistry, University of California, Los Angeles, Los Angeles, California 90095-1569, United States
- Ellen M. Sletten Department of Chemistry and Biochemistry, University of California, Los Angeles, Los Angeles, California 90095-1569, United States; orcid.org/ 0000-0002-0049-7278

Complete contact information is available at: https://pubs.acs.org/10.1021/acs.jpclett.2c01504

Notes

The authors declare no competing financial interest.

ACKNOWLEDGMENTS

A.V.S., A.S.H., T.L.A., and J.R.C. acknowledge funding from the National Science Foundation, Career Grant (CHE-1945572), and the ACS Petroleum Research Fund (62717-DNI6). H.H.L. and E.M.S. acknowledge National Institutes of Health grant number 5R01GM135380.

REFERENCES

- (1) Cui, J.; Beyler, A. P.; Bischof, T. S.; Wilson, M. W. B.; Bawendi, M. G. Deconstructing the photon stream from single nanocrystals: from binning to correlation. *Chem. Soc. Rev.* **2014**, *43*, 1287–1310.
- (2) Schlegel, G.; Bohnenberger, J.; Potapova, I.; Mews, A. Fluorescence Decay Time of Single Semiconductor Nanocrystals. *Phys. Rev. Lett.* **2002**, *88*, 137401.
- (3) Rigler, R.; Elson, E. S.Fluorescence Correlation Spectroscopy: Theory and Applications; Springer Series in Chemical Physics, Vol. 65; Springer-Verlag: Berlin Heidelberg, 2001.
- (4) Kliger, D. S.; Lewis, J. W.; Randall, C. E. Polarized Light in Optics and Spectroscopy; Academic Press, Inc, 1990; DOI: 10.1016/C2009-0-22282-3.
- (5) Tokunaga, E.; Terasaki, A.; Kobayashi, T. Frequency-domain interferometer for femtosecond time-resolved phase spectroscopy. *Opt. Lett.* **1992**, *17*, 1131–1133.
- (6) Valeur, B.; Berberan-Santos, M. N.Molecular Fluorescence: Principles and Applications; Wiley-VCH, 2013.
- (7) Schlawin, F. Entangled photon spectroscopy. J. Phys. B 2017, 50, 203001.
- (8) Loumaigne, M.; Vasanthakumar, P.; Richard, A.; Débarre, A. Time-of-Flight Photon Spectroscopy: A Simple Scheme to Monitor Simultaneously Spectral and Temporal Fluctuations of Emission on Single Nanoparticles. *ACS Nano* **2012**, *6*, 10512–10523.
- (9) Crouch, C. H.; Sauter, O.; Wu, X.; Purcell, R.; Querner, C.; Drndic, M.; Pelton, M. Facts and Artifacts in the Blinking Statistics of Semiconductor Nanocrystals. *Nano Lett.* **2010**, *10*, 1692–1698.
- (10) Ambrose, W. P.; Moerner, W. E. Fluorescence spectroscopy and spectral diffusion of single impurity molecules in a crystal. *Nature* **1991**, 349, 225–227.
- (11) Atallah, T. L.; Sica, A. V.; Shin, A. J.; Friedman, H. C.; Kahrobai, Y. K.; Caram, J. R. Decay-Associated Fourier Spectroscopy: Visible to Shortwave Infrared Time-Resolved Photoluminescence Spectra. *J. Phys. Chem. A* **2019**, *123*, 6792–6798.
- (12) Caram, J. R.; Bertram, S. N.; Utzat, H.; Hess, W. R.; Carr, J. A.; Bischof, T. S.; Beyler, A. P.; Wilson, M. W. B.; Bawendi, M. G. PbS Nanocrystal Emission Is Governed by Multiple Emissive States. *Nano Lett.* **2016**. *16*, 6070–6077.
- (13) Ellis, J. D.; Spronck, J. W.; Joo, K.-N.; van Kan, P. J. M.; Schmidt, R. H. M. Simple heterodyne laser interferometer with subnanometer periodic errors. *Opt. Lett.* **2009**, *34*, 386–388.

- (14) Hou, W.; Wilkening, G. Investigation and compensation of the nonlinearity of heterodyne interferometers. *Precision Eng.* **1992**, *14*, 91–98.
- (15) Xie, Y.; Wu, Y. Zeeman laser interferometer errors for high-precision measurements. *Appl. Opt.* **1992**, *31*, 881–884.
- (16) Fu, H.; Wu, G.; Hu, P.; Tan, J.; Ding, X. Thermal Drift of Optics in Separated-Beam Heterodyne Interferometers. *IEEE Trans. Instrum. Meas.* **2018**, *67*, 1446–1450.
- (17) Scully, M. O.; Zubairy, M. S.Quantum Optics; Cambridge University Press, 1997; DOI: 10.1017/CBO9780511813993.
- (18) Day, R. A.; Sletten, E. M. Experimental Perspectives on Direct Visualization of Endosomal Rupture. *ChemBioChem.* **2021**, 22, 3277–3282.
- (19) Sutton, E. J.; Henning, T. D.; Pichler, B. J.; Bremer, C.; Daldrup-Link, H. E. Cell tracking with optical imaging. *Eur. Radiol.* **2008**, *18*, 2021–2032.
- (20) Lim, I.; Vian, A.; van de Wouw, H. L.; Day, R. A.; Gomez, C.; Liu, Y.; Rheingold, A. L.; Campàs, O.; Sletten, E. M. Fluorous Soluble Cyanine Dyes for Visualizing Perfluorocarbons in Living Systems. *J. Am. Chem. Soc.* **2020**, *142*, 16072–16081.
- (21) Mosier-Boss, P. A.; Lieberman, S. H.; Newbery, R. Fluorescence Rejection in Raman Spectroscopy by Shifted-Spectra, Edge Detection, and FFT Filtering Techniques. *Appl. Spectrosc.* **1995**, 49, 630–638.
- (22) Rossi, T. M.; Warner, I. M. Fourier Transform Filtering of Two-Dimensional Fluorescence Data. *Appl. Spectrosc.* **1984**, *38*, 422–429.
- (23) Lieber, C. A.; Mahadevan-Jansen, A. Automated Method for Subtraction of Fluorescence from Biological Raman Spectra. *Appl. Spectrosc.* **2003**, *57*, 1363–1367.
- (24) Candeo, A.; Nogueira de Faria, B. E.; Erreni, M.; Valentini, G.; Bassi, A.; de Paula, A. M.; Cerullo, G.; Manzoni, C. A hyperspectral microscope based on an ultrastable common-path interferometer. *APL Photonics* **2019**, *4*, 120802.
- (25) Fernée, M. J.; Plakhotnik, T.; Louyer, Y.; Littleton, B. N.; Potzner, C.; Tamarat, P.; Mulvaney, P.; Lounis, B. Spontaneous spectral diffusion in CdSe quantum dots. *J. Phys. Chem. Lett.* **2012**, 3, 1716–1720.
- (26) Griffiths, P. R.; de Haseth, J. A.Fourier Transform Infrared Spectrometry, 2nd ed.; Wiley, 2007; pp 1-529,